Table 2. Complications in 39 patients treated with HBO/IAR therapy

Fever (≥37°C)	53.8%
Gastrointestinal complaints	
Appetite loss	64.1%
Constipation	53.8%
Nausea	15.4%
Hematological toxicity	
Grade 0	7.7%
Grade 1	15.4%
Grade 2	43.6%
Grade 3	30.8%
Grade 4	2.5%
Hepatic toxicity	
Grade 0	46.1%
Grade 1	20.5%
Grade 2	18.0%
Grade 3	15.4%
Grade 4	0%
Severe tympanitis	2.5%
Psychological depression	2.5%

complaints were frequent complications among all 39 patients (Table 2). Hair loss was limited to the irradiated field in all patients. Twenty-one patients (53.8%) developed fever (over 37°C) due to IFN-beta. Twenty-five (64.1%) and 21 patients (53.8%) complained of appetite loss and constipation, respectively. Only six patients (15.4%) complained of nausea. With respect to hematological toxicity, WHO grade 2 (WBC: 2.0–2.9 × 10^3/mm^3, Platelet: 50–74 × 10^3/mm^3 and/or Hemoglobin: 8.0–9 g/dl) frequently appeared. Grade 0 hepatic toxicity (SGOT or SGPT: ≤1.25 × maximal normal range) was the most frequent and renal toxicity was absent. In all 30 patients (76.9%) either maintained or increased the KPS value. The mean of the KPS values before and after HBO/IAR for all patients were 64 ± 14 and 65 ± 18, respectively (not significant).

Therapeutic efficacy

In 30 patients excluded nine in whom two withdrew from HBO/IAR therapy and then received the other chemotherapy and seven who underwent total removal, the response rates (CR + PR) were evaluated. The response rates of the glioblastoma and anaplastic astrocytoma patients and the overall were 50% (10/20), 30% (3/10) and 43% (13/30) (Table 3 and Figure 1A–D). Only two patients showed PD; one had not received any second-line chemotherapy after withdrawing HBO/IAR therapy due to grade 4 hematological toxicity and other had anaplastic

Table 3. Responses to HBO/IAR therapy in 30 patients*

	CR (%)	PR (%)	NC (%)	PD (%)
Glioblastoma (n = 20)	10	40	45	5
Anaplastic astrocytoma (n = 10)	0	30	60	10
Overall (n = 30)	7	36	50	7

*Two patients who withdrew from HBO/IAR therapy and then received the other chemotherapy and seven who underwent total resection were excluded.

astrocytoma which rapidly infiltrated multilobes like gliomatosis cerebri in MR images after HBO/IAR therapy.

In 30 patients excluded nine in whom two withdrew from HBO/IAR therapy and then received the other chemotherapy and seven who underwent total removal, means of age, KPS and tumor size were 53.4 years old, 63.7% and 24.9 cm^3, respectively. Differences of response rates in age (≥54 vs. ≤53), KPS (≥70 vs. ≤60), histological type (glioblastoma vs. anaplastic astrocytoma) and tumor size (≥24.9 vs. <24.9) were not significant. There were no significant differences among the main tumor sites or among operation types (Table 4).

In 37 patients excluding two who withdrew from HBO/IAR therapy and then received the other chemotherapy, TTP was evaluated. The median TTP for patients with glioblastoma, those with anaplastic astrocytoma and overall, were 38, 56 and 43 weeks, respectively (Figure 2). When limited to the 27 glioblastoma patients excluding two who withdrew from HBO/IAR therapy and then received the other chemotherapy, the median TTPs for non-responders (n = 10) with NC or PD, responders (n = 10) who achieved CR or PR, and those who underwent total removal followed by HBO/IAR therapy (n = 7) were 17, 43 and 49 weeks, respectively. The TTP value for non-responders was significantly shorter than those patients whose tumor was totally removed at surgery and then underwent HBO/IAR therapy. The difference in the TTP between non-responders and responders was not significant (Figure 3).

Thirty patients underwent the complete schedule of HBO/IAR therapy as well as retaining a KPS of greater than 50% after the therapy (Table 1). Of 23 patients with glioblastoma, 13 received maintenance therapy using IFN-beta and ACNU after HBO/IAR therapy. The median TTP for patients treated with

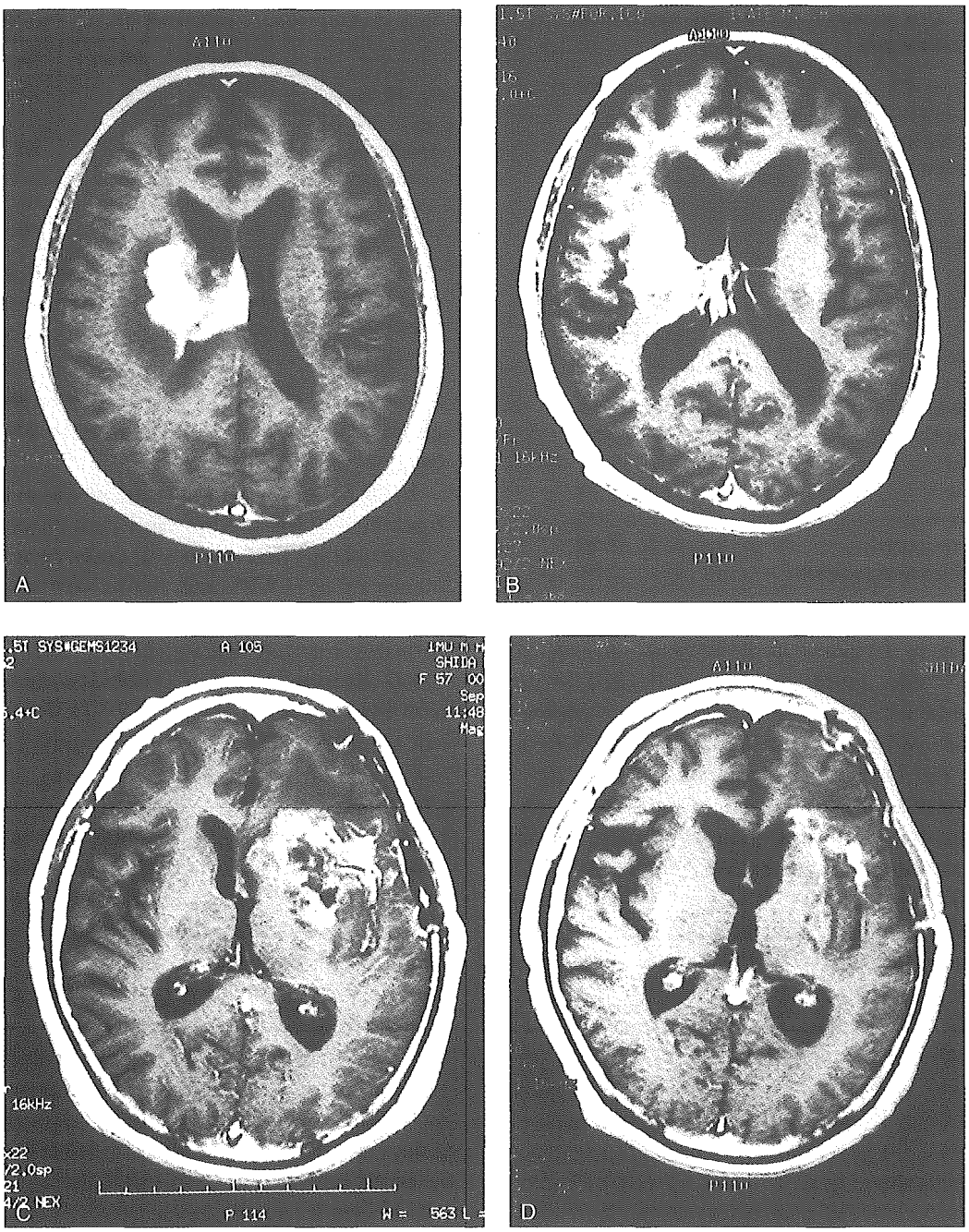

Figure 1. Gadolinium-enhanced T1 weighted MR images of patients showing a complete (A, B) and partial response (C, D). Before (A, C) and after HBO/IAR therapy (B, D). A and B, the patient of no. 16; C and D, the patient of no. 17 in Table 1.

maintenance therapy ($n = 13$) and without maintenance therapy ($n = 10$) were 49 and 31 weeks, respectively. Although a trend to increased TTP was seen in patients treated with maintenance therapy, the difference between the two groups was not significant ($p = 0.07$) (Figure 4). In total 30 patients, the TTP for patients ($n = 17$) treated with maintenance therapy was significantly prolonged than that for patients ($n = 13$) without maintenance therapy ($p = 0.04$) (not shown in Figure).

Discussion

Although IAR therapy has been established as one of the standard adjuvant chemotherapies for malignant

Table 4. Incidence of responses among prognostic factors before HBO/IAR therapy in 30 patients*

Prognostic factors	Incidence of CR or PR	*p*-value
Age		0.15
≥54 ($n = 14$)	57.1% (8/14)	
≤53 ($n = 16$)	45.4% (5/11)	
KPS (%)		0.31
≥70 ($n = 13$)	53.8% (7/13)	
≤60 ($n = 17$)	35.3% (6/17)	
Histology		0.30
GB ($n = 20$)	50.0% (10/20)	
AA ($n = 10$)	30.0% (3/10)	
Tumor size (cm^3)		0.60
≥24.9 ($n = 10$)	50.0% (5/10)	
<24.9 ($n = 20$)	40.0% (8/20)	
Tumor sites		0.65
Right side ($n = 6$)	33.3% (2/6)	
Left side ($n = 9$)	55.6% (5/9)	
Deep regions ($n = 15$)	40.0% (6/15)	
Extent of removal		0.93
Subtotal ($n = 6$)	50.0% (3/6)	
Partial ($n = 10$)	40.0% (4/10)	
Biopsy ($n = 14$)	42.9% (6/14)	

KPS – Karnofsky performance scale; GB – glioblastoma; AA – anaplastic astrocytoma. *Two patients who withdrew from HBO/IAR therapy and then received the other chemotherapy and seven who underwent total resection were excluded.

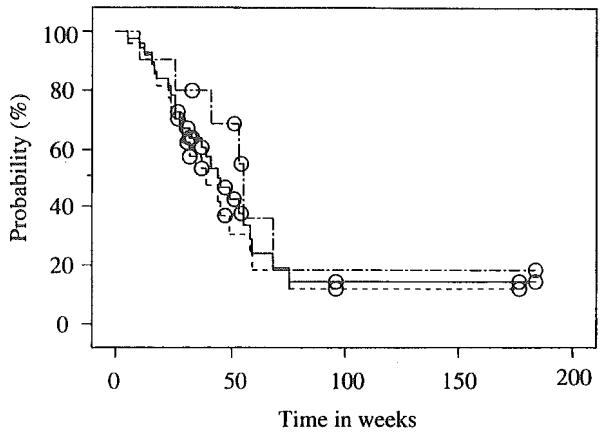

Figure 2. TTP for patients with glioblastoma (dashed line), patients with anaplastic astrocytoma (chain line) and overall (solid line). ○, patients without recurrence.

glioma in Japan, few previous studies have been reported. Shibata [21] previously reported IAR therapy alone for malignant gliomas. In his study, the response rate was 33.3%. Although total doses of IFN-beta, ACNU and radiation applied to patients in the present study were similar to those of Shibata, the present

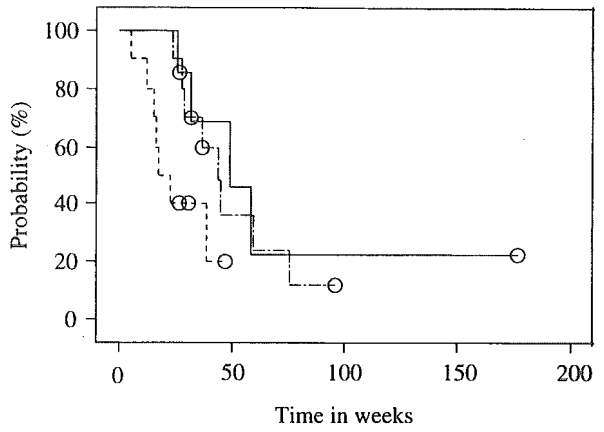

Figure 3. TTP of 27 patients with glioblastoma who were non-responders, responders, or who underwent total removal followed by HBO/IAR therapy. Log rank *p*-value for non-responders *versus* responders, 0.09; for non-responders *versus* total removal of tumor, 0.04. Solid line, total removal of tumor; chain line, responders; dashed line, non-responders. ○, patients without recurrence.

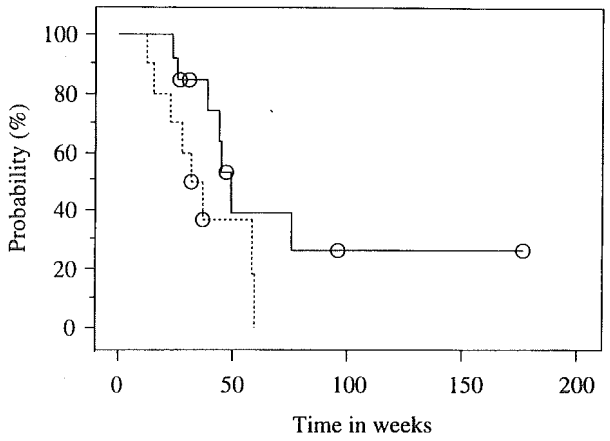

Figure 4. TTP of 23 patients with glioblastoma who were treated with maintenance therapy or who were not treated with any additional therapy after HBO/IAR therapy. Log rank *p*-values for treated patients *versus* non-treated patients, 0.07. Solid line, patients treated with maintenance therapy; dashed line, patients treated without maintenance therapy.

response rates (Table 3) were considerably better than those of Shibata. Yoshida et al. [3] reported that the complete remission rate for malignant glioma patients treated with IAR alone was 23%. However, our findings could not be compared with those of Yoshida et al. because their patients showing complete remission included patients whose tumor disappeared radiologically by surgery. A recent report by Wakabayashi et al. [8] on IMR therapy alone using IFN-beta, MCNU which is better able to enter brain tumors than ACNU,

and radiation has indicated that the response rate for glioblastoma was 50%. However, in their report, the relationship between the extent of tumor reduction by surgery and the therapeutic response was not defined in the criteria. In the present study, the assessments of therapeutic response did not include the contributions of tumor reduction by surgery.

Our preliminary study confirmed that pO_2 in glioblastoma tissue retains a high level for 15 min after HBO *in vivo* [20]. It is, therefore, suggested that the response to radiation therapy would be improved if it is applied within 15 min after HBO. Oxygenation using HBO would also enhance sensitivity to chemotherapy, because hypoxic conditions in the tissue compromise the chemotherapeutic potential of almost all agents [22–24]. In HBO/IAR therapy, there might also be a possibility that sensitivity to chemotherapy was enhanced by HBO. However, our preliminary study showed that the high pO_2 level achieved immediately after HBO gradually decreased to the pre-HBO level within approximately 40 min [20]. Since both ACNU and IFN-beta at 2 h were administered after HBO in the present study, it was suggested that an improvement in the chemotherapeutic potential would be insignificant even though an enhancement of the chemosensitivity existed. Although the toxicity of HBO/IAR was permissible as shown in Table 2, it was not clarified how frequent white matter injury, e.g., ischemic change and delayed radiation necrosis [25], due to radiation following HBO presents in the future. However, we speculate that the frequency will not differ significantly when compared with patients administered radiation without HBO, because the oxygen consumption rate after HBO was reportedly higher in normal white matter than in tumor tissue [19].

Several studies reported that prognostic factors such as age, performance status, histology, tumor sites and extent of tumor removal affect survival [3,26–28]. Age, KPS, and extent of tumor removal are also predictors of radiation response to glioblastomas [29]. The present study found no significant differences in the response rates with respect to age, KPS, histological type, tumor size, tumor site and operation type (Table 4). The present results suggest that HBO/IAR therapy also has good potential for patients with poor prognostic factors. The results of a good response to glioblastoma were compatible with previous findings where the response was affected by the tumor proliferation potential [3,30]. The reason for the good response in older patients is unknown, whereas no significant differences in the responses in the KPS, tumor size, tumor site and operation type may have resulted from the improved radiosensitivity by HBO. The pO_2 level in large residual tumors after biopsy or after partial removal must be generally low because of the inadequate blood flow from the compression of capillary vessels caused by both the mass effect and peritumoral edema itself [31–33]. It is suggested that HBO did not lead to improve radiosensitivity of only small residual tumors but also large residual tumors, because various size glioblastomas that were not resected retained high pO_2 levels greater than the 30 mmHg of maximal radiosensitivity within 15 min after HBO in our preliminary study [20]. Close associations exist among performance status, tumor size, tumor sites and operation type, because the residual tumor size determined by operation type affects patient performance and is affected by tumor site. Improvement in radiosensitivity of large residual tumors would contribute to increased response rates of both patients with poor performance and with tumors in the deep regions, e.g., basal ganglia, insular cortex and corpus callosum.

Adjuvant therapy must be applied over a short period, have low toxicity, and maintain the performance status, so that patients can be rehabilitated with a good quality of life as soon as possible. In the present study, the duration required for the initial treatment containing HBO/IAR therapy (68 ± 14 days) was shorter than that associated with adjuvant chemotherapy, in which a course of radiation therapy was followed by a course of chemotherapy [2]. Toxicity of HBO/IAR was permissible. Furthermore, 76.9% of patients either maintained or increased the KPS value during HBO/IAR therapy. We speculated that the reasons for maintaining performance during the HBO/IAR therapy were the short duration, permissible toxicity, and high potential for a good therapeutic response. Therefore, these findings suggested that HBO/IAR therapy might be beneficial for especially patients with poor prognostic factors.

Although HBO/IAR showed good responses to residual tumors, the median TTP of HBO/IAR therapy was unsatisfactory: 38 weeks for glioblastoma, 56 weeks for anaplastic astrocytoma and 43 weeks overall (Figure 2). The prolonged TTP induced by the response to HBO/IAR therapy was only 26 weeks (43 weeks for responders minus 17 weeks for non-responders) (Figure 3). These results suggested that the therapeutic response to initial treatment does not directly correlate to prognoses. One study proposed that the survival period prolonged by cancer therapy consists of the periods required for tumor reduction by treatment, tumor dormancy by cytostasis, and a return

to pretreatment status due to tumor re-growth or recurrence [34]. The TTP is equivalent to both periods required for tumor reduction by treatment and tumor dormancy. Accordingly, prolonging the period of tumor dormancy increases the survival period. The results of the present maintenance therapy were unsatisfactory to prolong the dormant period of glioblastomas, although the follow-up period was short. Effective maintenance therapies or other strategies following HBO/IAR therapy for glioblastoma patients are required to prolong the period of tumor dormancy.

In conclusion, HBO/IAR therapy could be applied to especially patients with poor prognostic factors, because of its short treatment period, its permissible toxicity and identical response to patients with good prognostic factors. Finally, further studies should be performed by cooperative groups using a prospective randomized trial to strictly confirm that HBO/IAR therapy was beneficial for patients with malignant glioma.

Acknowledgements

This study was supported in part by a Grant-in-Aid for Advanced Medical Science Research from the Ministry of Science, Education, Sports and Culture, Japan.

References

1. Ammirati M, Vick N, Liao YL, Ciric I, Mikhael M: Effect of extent of surgical resection on survival and quality of life in patients with supratentorial glioblastoma and anaplastic astrocytomas. Neurosurgery 21: 201–206, 1987
2. Beppu T, Yoshida Y, Arai H, Wada T, Suzuki M, Ogawa A, Hakozaki S, Kubo N: A phase II study of nimustine hydrochloride, cisplatin, and etoposide combination chemotherapy for supratentorial malignant gliomas. J Neuro-Oncol 49: 213–218, 2000
3. Yoshida J, Kajita Y, Wakabayashi T, Sugita K: Long-term follow-up results of 175 patients with malignant glioma: importance of radical tumour resection and postoperative adjuvant therapy with interferon, ACNU and radiation. Acta Neurochir (Wien) 127: 55–59, 1994
4. Gresser I, Maury C, Brouty-Boye D: Mechanism of the antitumour effect of interferon in mice. Nature 239(5368): 167–168, 1972
5. Nagai M, Arai T: Clinical effect of interferon in malignant brain tumours. Neurosurg Rev 7(1): 55–64, 1984
6. Yamamoto SH, Tanaka H, Kanamori M, Nobuhara M, Namba M: *In vitro* studies on potentiation of cytotoxic effects of anticancer drugs by interferon on a human neoplastic cell line (HeLa). Cancer 20: 131–138, 1983
7. Yoshida J, Kato K, Wakabayashi T, Enomoto H, Inoue I, Kageyama N: Antitumor activity of interferon-beta against malignant glioma in combination with chemotherapeutic agent of nitrosourea (ACNU). In: Cantell K, Schellekens H (eds) The Biology of the Interferon System. Martinus Nijhoff Publishers, Dordrecht, 1986, pp 399–406
8. Wakabayashi T, Hatano N, Kajita Y, Yoshida T, Mizuno M, Taniguchi K, Ohno T, Nagasaka T, Yoshida J: Initial and maintenance combination treatment with interferon-beta, MCNU (Ranimustine), and radiotherapy for patients with previously untreated malignant glioma. J Neuro-Oncol 49: 57–62, 2000
9. Hatano N, Wakabayashi T, Kajita Y, Mizuno M, Ohno T, Nakayashiki N, Takemura A, Yoshida J: Efficacy of post operative adjuvant therapy with human interferon beta, MCNU and radiation (IMR) for malignant glioma: comparison among three protocols. Acta Neurochir (Wien) 142: 633–638, 2000
10. Wakabayashi T, Yoshida J, Mizuno M, Kito A, Sugita K: Effectiveness of interferon-beta, ACNU, and radiation therapy in pediatric patients with brainstem gliomas. Neurol Med Chir (Tokyo) 32: 942–946, 1992
11. Dowling S, Fischer JJ, Rockwell S: Fluosol and hyperbaric oxygen as an adjunct to radiation therapy in the treatment of malignant gliomas: a pilot study. Biomater Artif Cells Immobilization Biotechnol 20: 903–905, 1992
12. Horsman MR: Nicotinamide and other benzamide analogs as agents for overcoming hypoxic cell radiation resistance in tumours. A review. Acta Oncol 34: 571–587, 1995
13. Kohshi K, Kinoshita Y, Terashima H, Konda N, Yokota A, Soejima T: Radiotherapy after hyperbaric oxygenation for malignant gliomas: a pilot study. J Cancer Res Clin Oncol 122: 676–678, 1996
14. Thomlinson RH, Gray LH: The histological structure of some human lung cancers and the possible implications for radiotherapy. Br J Cancer 9: 539–549, 1995
15. Gray LH, Cogner AD, Ebert M, Hornsey A, Scott OCA: The concentration of oxygen dissolved in tissues at the time of irradiation as a factor in radiotherapy. Br J Radiol 26: 638–648, 1953
16. Chang CH: Hyperbaric oxygen and radiation therapy in the management of glioblastoma. Natl Cancer Inst Monogr 46: 163–169, 1977
17. Kohshi K, Kinoshita Y, Imada H, Kunugita N, Abe H, Terashima H, Tokui N, Uemura S: Effects of radiotherapy after hyperbaric oxygenation on malignant gliomas. Br J Cancer 80: 236–241, 1999
18. Saunders M, Dische S: Clinical results of hypoxic cell radiosensitization from hyperbaric oxygen to accelerated radiotherapy, carbogen and nicotinamide. Br J Cancer 74 (Suppl XXVII): 271–278, 1996
19. Jamieson D, van den Brenk HAS: Measurement of oxygen tensions in cerebral tissues of rats exposed to high pressures of oxygen. J Appl Physiol 18: 869–876, 1963
20. Beppu T, Kamada K, Yoshida Y, Arai H, Ogasawara K, Ogawa A: Change of oxygen pressure in glioblastoma tissue under various conditions. J Neuro-Oncol 43: 47–52, 2002
21. Shibata S: Combination therapy with interferon-beta, ACNU and radiation (IAR) for malignant gliomas. Kiso to Rinsho 23: 321–324, 1989 (in Japanese)

ELSEVIER

Imaging

THREE-DIMENSIONAL ANISOTROPY CONTRAST IMAGING OF GLIOMATOSIS CEREBRI: TWO CASE REPORTS

Takashi Inoue, M.D., Kuniaki Ogasawara, M.D., Takaaki Beppu, M.D., and Akira Ogawa, M.D.
Department of Neurosurgery, Iwate Medical University School of Medicine, Morioka, Iwate, Japan

Inoue T, Ogasawara K, Beppu T, Ogawa A. Three-dimensional anisotropy contrast imaging of gliomatosis cerebri: two case reports. Surg Neurol 2004;62:151–155.

BACKGROUND
Magnetic resonance imaging (MRI) can provide a preoperative diagnosis of gliomatosis cerebri, but the findings sometimes do not correspond with the clinical symptoms or histologic findings.

CASE DESCRIPTION
Three-dimensional anisotropy contrast (3DAC) imaging was used to assess damage to the neuronal fibers in two patients with gliomatosis cerebri who presented with only mental deterioration. Conventional MRI depicted markedly abnormal findings consisting of widespread areas of abnormally high signal intensity in the corpus callosum and in the bilateral white matter in both cases. In contrast, 3-D AC imaging showed no abnormality except for small dark areas in the corpus callosum or white matter.

CONCLUSION
3-D AC imaging provides more accurate information about damage to the neuronal fibers in cases of gliomatosis cerebri than other MRI techniques.

KEY WORDS
Gliomatosis cerebri, neuronal fiber, three-dimensional anisotropy contrast.

Gliomatosis cerebri is a rare variant of glioma characterized by diffuse proliferation of glial elements infiltrating normal nervous tissue with relative preservation of the underlying brain architecture [1,5,13]. The clinical manifestations include mental deterioration, personality change, and signs of increased intracranial pressure [4,8,14]. Disconnection syndrome may be detected in patients with infiltrating tumors involving the corpus callosum [12,17,19].

We treated 2 patients with gliomatosis cerebri who presented with only mental deterioration. Damage to the neuronal fibers was assessed using three-dimensional (3-D) anisotropy contrast (3DAC) imaging.

CASE REPORTS

PATIENT 1

A 48-year-old woman in good health suffered generalized tonic convulsion. On admission, general physical examination found no abnormalities. Neurologic examination identified no motor weakness, no sensory deficit, and neither apraxia nor agnosia. Testing of cognitive function demonstrated mental deterioration: verbal intelligence quotient (IQ) was 60 points and performance IQ was 58 points on the Wechsler Adult Intelligence Scale-Revised (WAIS-R) [21].

Magnetic resonance imaging (MRI) was performed with a Signa VH/i 3.0 T (General Electric Systems, Milwaukee, WI). Short inversion time inversion recovery (STIR) sequence was used for T2-weighted imaging with the following parameters: repetition time (TR) 5000 ms, echo time (TE) 25 ms, inversion time 140 ms, matrix 512 × 384, field of view (FOV) 240 mm, and 6 mm slice thickness. Diffusion-weighted (DW) imaging with motion providing gradients applied in three directions was also performed to investigate the neuronal fibers using the following parameters: TR 6000 ms, TE 80 ms, matrix 256 × 260, FOV 240 mm, 6 mm slice thickness, and b value 800 s/mm^2. The DW images were transferred to a personal computer and 3-D AC images were generated to visualize the directional-

Address reprint requests to: Takashi Inoue, M.D., Department of Neurosurgery, Iwate Medical University School of Medicine, 19-1 Uchimaru, Morioka, Iwate 020-8505, Japan.
Received August 7, 2002; accepted August 21, 2003.

360 Park Avenue South, New York, NY 10010–1710

0090-3019/03/$–see front matter
doi:10.1016/j.surneu.2003.08.031

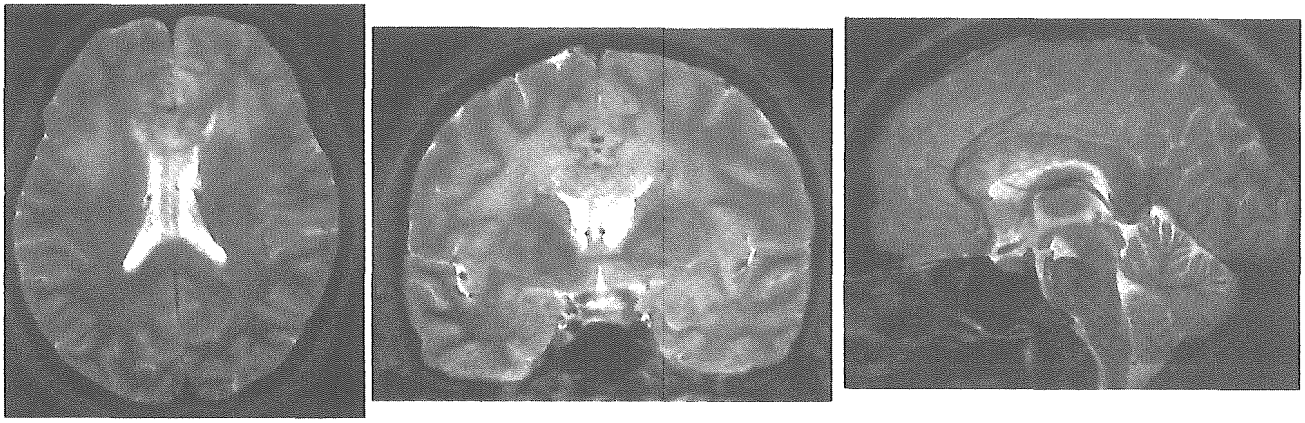

1 Axial (*left*), coronal (*center*), and sagittal (*right*) short inversion time inversion recovery images showing diffuse high-intensity lesions. Tumor invasion was apparently present in the enlarged corpus callosum, indicating a space-occupying lesion.

ity and damage in the neuronal fibers [10,16]. The STIR images depicted widespread areas of abnormally high signal intensity in the corpus callosum and in the white matter of the bilateral frontal and parietal lobes (Figure 1). In contrast, the 3DAC images showed no abnormality except for small dark areas in the corpus callosum (Figure 2).

Brain biopsy was performed by a stereotactic technique. Histologic examination of the specimens obtained from the corpus callosum showed diffuse glial infiltration. The majority of cells were spindle shaped with moderately differentiated neoplasticity and contained abnormally swollen nuclei (Figure 3). The histologic diagnosis was fibrillary astrocytoma.

PATIENT 2

A 68-year-old woman was transferred to our hospital after presenting with complaints of headaches. Computed tomography of the head revealed diffuse areas of abnormally low density. On admission, general physical examination found no abnormalities. Neurologic examination identified no motor weakness, no sensory deficit, and neither apraxia nor agnosia. Testing of cognitive function demonstrated mental deterioration: verbal IQ was 86 points and performance IQ was 61 points on the WAIS-R.

The STIR images showed widespread areas of abnormally high signal intensity in the splenium

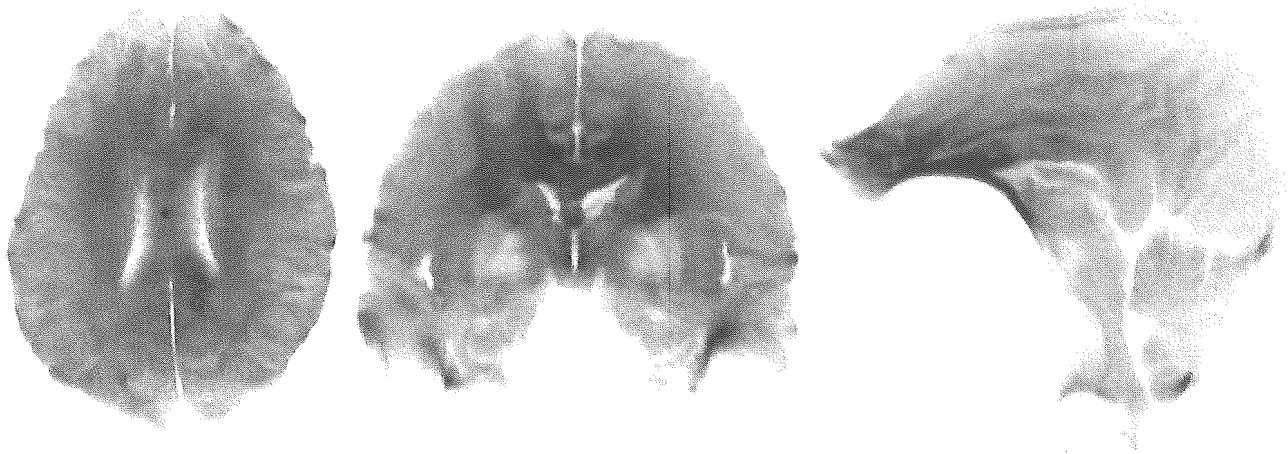

2 Axial (*left*), coronal (*center*), and sagittal (*right*) three-dimensional anisotropy contrast images. Neuronal fibers running in the superior-inferior, left-right, or anterior-posterior directions are assigned red, green, or blue, respectively. Mixed colors indicate oblique orientation of the neuronal fibers. The damaged fibers appear as dark areas, whereas the green area indicates that the neuronal fibers were running left to right or right to left in the corpus callosum. Image distortion was caused by a susceptibility artifact in the sagittal image.

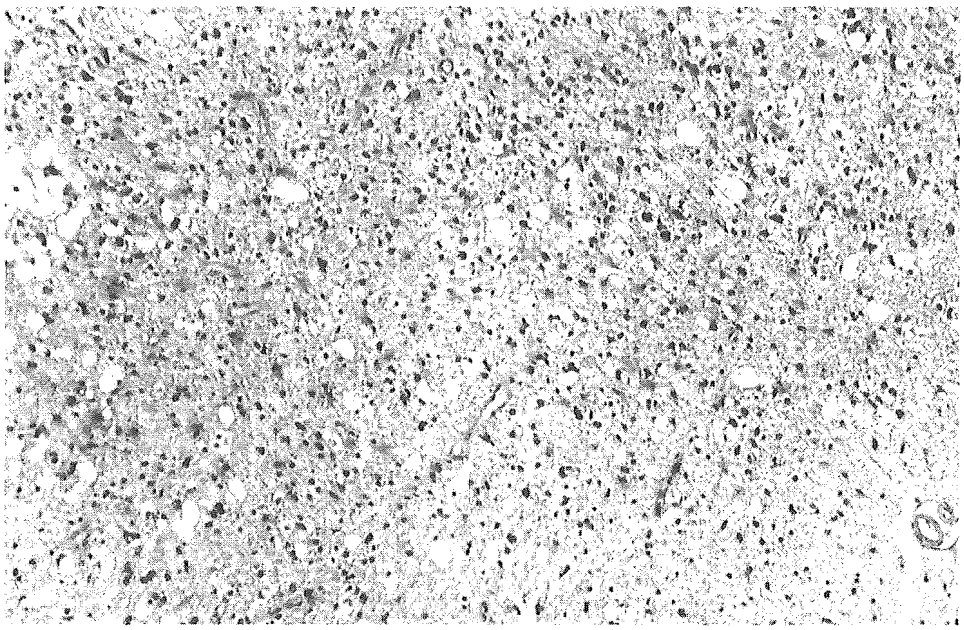

3 Photomicrograph of the specimen from the corpus callosum revealing increased numbers of glial cells (H&E; original magnification, × 100).

and in the white matter of the bilateral occipital and frontal lobes (Figure 4 left). In contrast, the 3DAC images showed no abnormality except for the dark areas in the occipital lobe (Figure 4 right).

Brain biopsy was performed by a stereotactic technique. The histologic diagnosis was fibrillary astrocytoma.

DISCUSSION

MRI can confirm the preoperative diagnosis of gliomatosis cerebri [5–7,15,18], because T2- or proton density-weighted MRI demonstrates the lesions as abnormally high intensity areas. However, histologic examination shows that abnormal glial cells

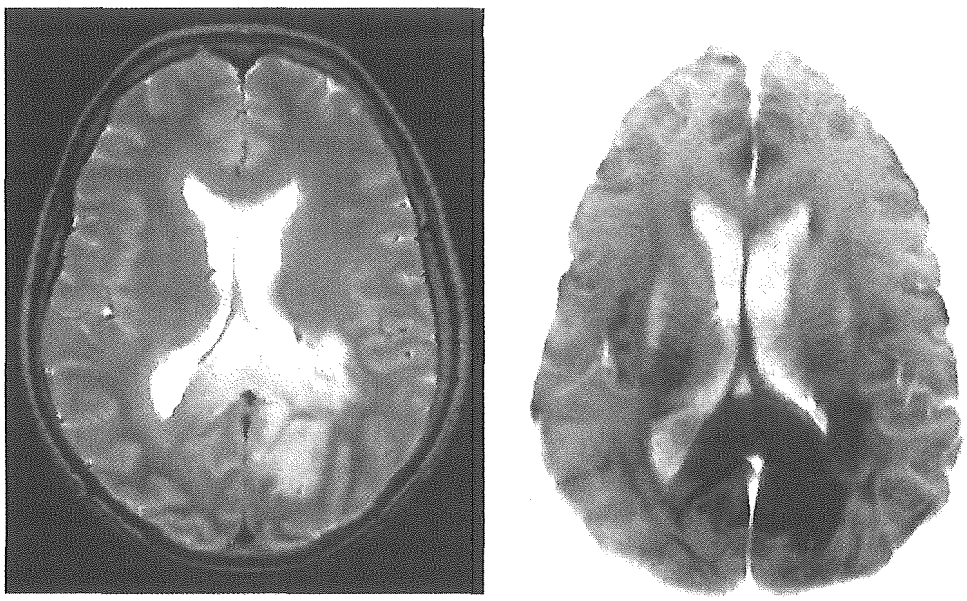

4 *Left:* Short inversion time inversion recovery image showing diffuse high-intensity lesions. Tumor invasion was apparently present in the enlarged corpus callosum, indicating a space-occupying lesion. *Right:* Three-dimensional anisotropy contrast image. Neuronal fibers running in the superior-inferior, left-right, or anterior-posterior directions are assigned red, green, or blue, respectively. Mixed colors indicate oblique orientation of the neuronal fibers. The corpus callosum appears as blue and green, which indicates that the neuronal fibers were not destroyed.

infiltrate the white matter along the anatomic pathways without destruction of the normal architecture [3,6,22]. The primary manifestations are not focal neurologic deficits as expected based on the findings of MRI but mental changes and increased intracranial pressure as expected based on the histologic features [1,2,14].

3DAC imaging is an established method to visualize directionality and damage in the neuronal fibers [9–11,20]. 3DAC imaging is useful to investigate the pathologic involvement of the pyramidal tract in patients with brain tumors [10]. In the present 2 cases, STIR imaging showed distinct abnormally high intensity areas in the corpus callosum and in the bilateral white matter, whereas 3DAC imaging showed no signal abnormality except for small dark areas in the corpus callosum or white matter. Clinically, both patients presented with no neurologic symptoms other than mental deterioration. Histologically, the specimens obtained from the corpus callosum showed existence of tumor cells. Although 3DAC imaging has some limitation to estimate the tumor existence, these findings suggest that 3DAC imaging provides more accurate information about damage to the neuronal fibers in patients with gliomatosis cerebri than other MRI methods.

This work was supported in part by Grants-in-Aid for Advanced Medical Science Research from the Ministry of Education, Culture, Sports, Science, and Technology, Japan.

REFERENCES

1. Artigas J, Cervos-Navarro J, Iglesias JR, Ebhardt G. Gliomatosis cerebri: clinical and histological findings. Clin Neuropathol 1985;4:135–48.
2. Couch JR, Weiss SA. Gliomatosis cerebri. Report of four cases and review of the literature. Neurology 1974;24:504–11.
3. Cummings TJ, Hulette CM, Longee DC, Bottom KS, McLendon RE, Chu CT. Gliomatosis cerebri: cytologic and autopsy findings in a case involving the entire neuraxis. Clin Neuropathol 1999;18:190–7.
4. Dickson DW, Horoupian DS, Thal LJ, Lantos G. Gliomatosis cerebri presenting with hydrocephalus and dementia. AJNR Am J Neuroradiol 1988;9:200–2.
5. Felsberg GJ, Silver SA, Brown MT, Tien RD. Radiologic-pathologic correlation. Gliomatosis cerebri. AJNR Am J Neuroradiol 1994;15:1745–53.
6. Freund M, Hahnel S, Sommer C, et al. CT and MRI findings in gliomatosis cerebri: a neuroradiologic and neuropathologic review of diffuse infiltrating brain neoplasms. Eur Radiol 2001;11:309–16.
7. Galatioto S, Marafioti T, Cavallari V, Batolo D. Gliomatosis cerebri. Clinical, neuropathological, immunohistochemical and morphometric studies. Zentralbl Pathol 1993;139:261–7.
8. Giovagnoli AR, Strada L, Pollo B, Boiardi A. Gliomatosis cerebri. Report of a case with isolated amnesic disorders. Ital J Neurol Sci 1992;13:503–6.
9. Igarashi H, Katayama Y, Tsuganezawa T, Yamamuro M, Terashi A, Owan C. Three-dimensional anisotropy contrast (3DAC) magnetic resonance imaging of the human brain: application to assess Wallerian degeneration. Intern Med 1998;37:662–8.
10. Inoue T, Shimizu H, Yoshimoto T. Imaging the pyramidal tract in patients with brain tumors. Clin Neurol Neurosurg 1999;101:4–10.
11. Inoue T, Shimizu H, Yoshimoto T, Kabasawa H. Spatial functional distribution in the corticospinal tract at the corona radiata: a three-dimensional anisotropy contrast study. Neurol Med Chir (Tokyo) 2001;41: 293–9.
12. Jinkins JR. The MR equivalents of cerebral hemispheric disconnection: a telencephalic commissuropathy. Comput Med Imaging Graph 1991;15:323–31.
13. Kannuki S, Hirose T, Horiguchi H, Kageji T, Nagahiro S. Gliomatosis cerebri with secondary glioblastoma formation: report of two cases. Brain Tumor Pathol 1998;15:111–6.
14. Kannuki S, Hondo H, Ii K, Hirose T, Matsumoto K. Gliomatosis cerebri with good prognosis. Brain Tumor Pathol 1997;14:53–7.
15. Koslow SA, Claassen D, Hirsch WL, Jungreis CA. Gliomatosis cerebri: a case report with autopsy correlation. Neuroradiology 1992;34:331–3.
16. Nakada T, Matsuzawa H, Kwee IL. Magnetic resonance axonography of the rat spinal cord. Neuroreport 1994;5:2053–6.
17. Plowman PN, Saunders CA, Maisey MN. Gliomatosis cerebri: disconnection of the cortical grey matter, demonstrated on PET scan. Br J Neurosurg 1998;12: 240–4.
18. Rippe DJ, Boyko OB, Fuller GN, Friedman HS, Oakes WJ, Schold SC. Gadopentetate-dimeglumine-enhanced MR imaging of gliomatosis cerebri: appearance mimicking leptomeningeal tumor dissemination. AJNR Am J Neuroradiol 1990;11:800–1.
19. Sidtis JJ, Sadler AE, Nass RD. Double disconnection effects resulting from infiltrating tumors. Neuropsychologia 1989;27:1415–20.
20. Watanabe T, Honda Y, Fujii Y, Koyama M, Matsuzawa H, Tanaka R. Three-dimensional anisotropy contrast magnetic resonance axonography to predict the prognosis for motor function in patients suffering from stroke. J Neurosurg 2001;94:955–60.
21. Wechsler D. Manual for the Wechsler Adult Intelligence Scale-Revised. New York: The Psychological Corporation, 1981.
22. Yanaka K, Kamezaki T, Kobayashi E, Matsueda K, Yoshii Y, Nose T. MR imaging of diffuse glioma. AJNR Am J Neuroradiol 1992;13:349–51.

COMMENTARY

The authors describe the use of 3-D anisotropy contrast (3 DAC) MRI to assess damage to the neuronal fibers in 2 patients with gliomatosis cerebri.

The useful use of 3 DAC highlights the trend toward 3-D MR axonography. Many reports have been published showing the usefulness of 3 DAC MRI to assess wallerian degeneration, involvement of py-

ramidal tract in patients with brain tumor, and demyelinating disease. The authors' report on 2 patients with gliomatosis cerebri, a rare disease, is another interesting application to study the gliomatosis cerebri. Their finding on 3 DAC is very interesting. However, does this justify believing there is no tumor along the tract? The diagnostic accuracy of 3 DAC MRI in their cases has not been studied by biopsy of areas, which were dark on 3 DAC MRI. It is an important imaging technique; however, its sensitivity is certainly less than perfect.

Clinical cranial MRI examinations include spin-echo T_1-weighted (T_1W), spin-echo T_2-weighted (T_2W) gradient echo pulse sequence, and fluid attenuation inversion recovery (FLAIR) pulse sequence. T_2W and FLAIR images generally depict more pathologic lesions than do spin-echo T_1W MR images. Gradient echo images are very useful to detect blood by-products, as well as calcification. Diffusion-weighted MRI (DWI) is widely used for the detection of acute ischemic stroke [1]. The contrast on a diffusion-weighted image of the brain is affected by the direction of white matter fiber pathways [2] to determine the direction and corresponding diffusivity of white fibers. The diffusion tensor imaging that characterizes anisotropic diffusion in 3D has to be performed [3]. Several methods that utilize diffusion anisotropy have been developed to depict the white matter fiber pathways [4]. Some of these methods use colors and the appearance of color image may depend on the choice of the computer display [2,5]. These techniques provide added information regarding the direction of white matter fibers so that structures that are indistinct on the spin-echo T_2W image may be delineated.

The white matter fiber pathways, in particular corpus callosum optic radiation, internal capsule and superior longitudinal fasciculus can be clearly identified. In addition, superposition of a spin-echo T2W MRI and a color-coded image, derived from three orthogonal diffusion-weighted images could show white matter tract architecture to further assess brain pathology.

Mahmood F. Mafee, M.D.
Department of Radiology
University of Illinois at Chicago
Chicago, Illinois

REFERENCES

1. Burdette JH, Elster AD, Ricci PE. Acute cerebral infarction: quantification of spin-density and T2 shine-through phenomena on diffusion-weighted MR images. Radiology 1999;212:333–9.
2. Tamura H, Takahashi S, Kurihara N, Yamada S, Hatazawa J, Okudera T. Practical visualization of internal structure of white matter for image interpretation: staining a spin-echo T2-weighted image with three echo-planar diffusion-weighted images. AJNR, Am J Neuroradiol 2003;24:401–9.
3. Shrager RJ, Basser PJ. Anisotropically weighted MRI. Magn Reson Med 1998;40:160–5.
4. Jones DK, Simmons A, Williams SC, Horsfield MA. Non-invasive assessment of axonal fiber connectivity in the human brain via diffusion tensor MRI. Magn Reson Med 1999;42:37–41.
5. Pajevic S, Pierpaoli C. Color schemes to represent the orientation of anisotropic tissues from diffusion tensor data: application to white matter fiber tract mapping in the human brain. Magn Reson Med 1999;42:526–40.

Available online at www.sciencedirect.com

SCIENCE DIRECT

ELSEVIER

Surgical Neurology 63 (2005) 56–61

SURGICAL NEUROLOGY

www.surgicalneurology-online.com

Imaging

Fractional anisotropy value by diffusion tensor magnetic resonance imaging as a predictor of cell density and proliferation activity of glioblastomas

Takaaki Beppu, MD[a,*], Takashi Inoue, MD[a], Yuji Shibata, PhD[b], Noriyuki Yamada, PhD[c], Akira Kurose, MD[b], Kuniaki Ogasawara, MD[a], Akira Ogawa, MD[a], Hiroyuki Kabasawa, DEng[d]

Departments of [a]Neurosurgery, [b]First Department of Pathology, and [c]Clinical Pathology, Iwate Medical University, Morioka 020-8505, Japan

[d]GE Yokogawa Medical Systems, Tokyo, Japan

Received 4 March 2003; accepted 12 February 2004

Abstract

Background: In vivo, water diffusion displays directionality due to presence of complex microstructural barriers in tissue. The extent of directionality of water diffusion can be expressed as a fractional anisotropy (FA) value using diffusion tensor magnetic resonance imaging (DTI). The FA value has been suggested as an indicator of the cell density of astrocytic tumors. The aim of the present study was to confirm beyond doubt that FA values indicate cell density even when limited in glioblastomas and to determine whether the FA value of a given patient predicts proliferation activity in the individual glioblastoma.

Methods: We performed DTI in 19 patients with glioblastoma and measured the FA values of tumor and normal brain regions prior to computed tomography–guided stereotactic biopsy. Differences in mean FA value between normal brain regions and glioblastoma lesion were compared. Cell density and MIB-1 indices were examined using tumor specimens obtained from biopsies. Correlation among FA values, cell density, and MIB-1 indices was also evaluated.

Results: The mean FA value significantly differed between normal brain regions and glioblastoma lesions. Positive correlation was observed between FA value and cell density ($r = 0.73$, $P < 0.05$) and between FA value and MIB-1 index ($r = 0.80$, $P < 0.05$).

Conclusions: Our results suggest that the FA value of glioblastoma as determined by DTI prior to surgery is a good predictor of cell density and, consequently, proliferation activity.

Keywords: Cell density; Diffusion tensor magnetic resonance imaging; Fractional anisotropy; Glioblastoma; Proliferation

1. Introduction

Essentially, the diffusion of water molecules displays microscopic random (Brownian) translational motion, and under these conditions, the molecular mobility of water is the same in all directions. In vivo, water diffusion takes on an abnormal motion due to hindrance by the presence of complex microstructural barriers in tissue, such as white matter tracts, cell membranes, and/or capillary vessels, and consequently the change in magnitude and directionality of water diffusion arises in a 3-dimensional space [2]. This directional variation is termed diffusion anisotropy. Diffusion tensor magnetic resonance imaging (DTI) provides quantitative information about the magnitude and directionality of water diffusion along a vector in a 3-dimensional space [4,6,17,26]. Evaluation of directionality of water diffusion using DTI has recently become available for visualization of cerebral fiber tracts [26] and demonstration of substantial differences among the various lesions of multiple sclerosis [1,7,8,24]. In DTI, a set of orthogonal vectors known as eigenvectors, which define the orientation of the principal axes of a diffusion ellipsoid in space, are

* Corresponding author. Tel.: +81 196 51 5111x6603; fax: +81 196 25 8799.

E-mail address: tbeppu@iwate-med.ac.jp (T. Beppu).

0090-3019/$ – see front matter © 2005 Elsevier Inc. All rights reserved.
doi:10.1016/j.surneu.2004.02.034

calculated from the diffusion tensor. The length of each vector is represented by corresponding eigenvalues. The fractional anisotropy (FA) is derived from eigenvectors for quantification of anisotropy. A FA value is calculated using the following formula based on eigenvalues in the diffusion tensor [2,18]:

$$FA = \sqrt{\frac{3}{2}} \frac{\sqrt{(\lambda_1 - \langle D \rangle)^2 + (\lambda_2 - \langle D \rangle)^2 + (\lambda_3 - \langle D \rangle)^2}}{\sqrt{\lambda_1^2 + \lambda_2^2 + \lambda_3^2}} \cdots \quad (1)$$

$$\langle D \rangle = \frac{1}{3}(\lambda_1 + \lambda_2 + \lambda_3) \cdots \quad (2)$$

where λ_1, λ_2, and λ_3 are the largest, intermediate, and smallest eigenvalues, respectively, of the diffusion tensor. The FA is expressed as a numerical value between 0 and 1 without a unit. A higher FA value implies a greater degree of anisotropic motion of water molecules.

Presurgical knowledge of the cell density and proliferation potential of the tumor tissue would have prognostic significance and help to elucidate the histologic characteristics in individual patients with astrocytic tumors. Water diffusion has been suggested to be affected by tumor cellularity in gliomas [22]. Our preliminary study suggested a correlation between the FA value and the tumor cell density or malignancy grades in astrocytic tumors [3], which led to the presumption that FA values also correlate with the cell proliferation activity of astrocytic tumors. To date, whether FA can act as an indicator of cell proliferation in astrocytic tumors is unknown. The quantitative estimation of cell density or proliferation is largely complicated by widely distributed values of differently graded astrocytic tumors when a study involves a group of mixed, differently graded tumors. To confirm whether FA values indicate cell density and proliferation activity of an astrocytic tumor group limited to 1 type, we examined the relationship among FA value, tumor cell density, and MIB-1 index, which is widely used as a quantitative information of cell proliferation [10,12,19,25] in glioblastomas alone.

2. Materials and methods

2.1. Patient population

The study protocol was approved by the Ethics Committee of Iwate Medical University (Morioka, Japan). The patients recruited to this study were admitted to the Department of Neurosurgery, Iwate Medical University, between September 2000 and December 2002. Entry criteria for this study were as follows: (A) adult patients who were diagnosed with supratentorial glioblastoma; (B) patients whose tumor was primarily in the cerebral white matter, except for the basal ganglia, corpus callosum, ventricle, and brain stem; (C) patients who received routine magnetic resonance imaging (MRI) and DTI within the 2 weeks prior to computed tomography–guided stereotactic biopsy; and (D) informed written consent to participate. Diagnosis was based on the histologic features of specimens obtained from a stereotactic biopsy according to the World Health Organization classification [13]. A total of 19 patients (11 males and 8 females; mean age, 58.9 years; age range, 28-77 years) participated. The main tumor sites were the frontal lobe in 6 patients, parietal lobe in 7, temporal lobe in 5, and occipital lobe in 1.

2.2. Measurement of FA value

All routine MRI and DTI scans were performed using a 3.0 T MRI system (Signa VH/I, GE Medical Systems, Milwaukee, WI) with a standard head coil. A spin echo–type echo planar imaging sequence with diffusion gradients applied in 6 directions was used for the diffusion tensor imaging: repetition time 10,000 ms, echo time 84 ms, matrix 256 × 260, field of view 240 mm^2, 6 mm thickness, 2 mm gap, b factors 800 s/mm^2. All patients also underwent conventional spin echo T1- and T2-weighted imaging prior to DTI and T1-weighted imaging with contrast medium after DTI. All image analysis after processing was performed on a scanner console using a subprogram of the Functool image analysis software (GE Medical Systems, Buc, France) modified by one of the investigators (HK).

The region of interest (ROI) was determined on a slice showing maximal tumor size in T1-weighted imaging with contrast medium, because the tumors of all patients were detected as enhancing lesions. Where possible, the ROI was placed at the enhancing central region of the tumor. If central necrosis was evident, the ROI was placed on a ring-enhancing region of the tumor containing more metabolically active sites than the central region (Fig. 1A). The ROI was also placed in subcortical normal white matter (NWM) where no abnormalities on T2-weighted MRI were detected. When the tumor was sited in the frontal lobe or anterior half of the temporal lobe, the ROI was placed in subcortical white matter of the contralateral occipital lobe. On the other hand, the ROI was placed in subcortical white matter of the contralateral frontal lobe when the tumor was situated in the parietal lobe, the occipital lobe, or the posterior half of the temporal lobe. If the tumor was not in or had not infiltrated into the corpus callosum on T2-weighted MRI, the ROI was placed at the genu or splenium of the corpus callosum. When the tumor was sited in the frontal lobe or anterior half of the temporal lobe, the ROI was placed in the splenium, whereas the ROI was placed in the genu when the tumor was situated in the parietal lobe, the occipital lobe, or the posterior half of the temporal lobe. ROIs were automatically transferred onto the coregistered FA maps constructed from DTI (Fig. 1B, C). The FA values were then calculated for each patient using the modified Functool image analysis software. The FA value was identified as a mean of values derived for every pixel in a

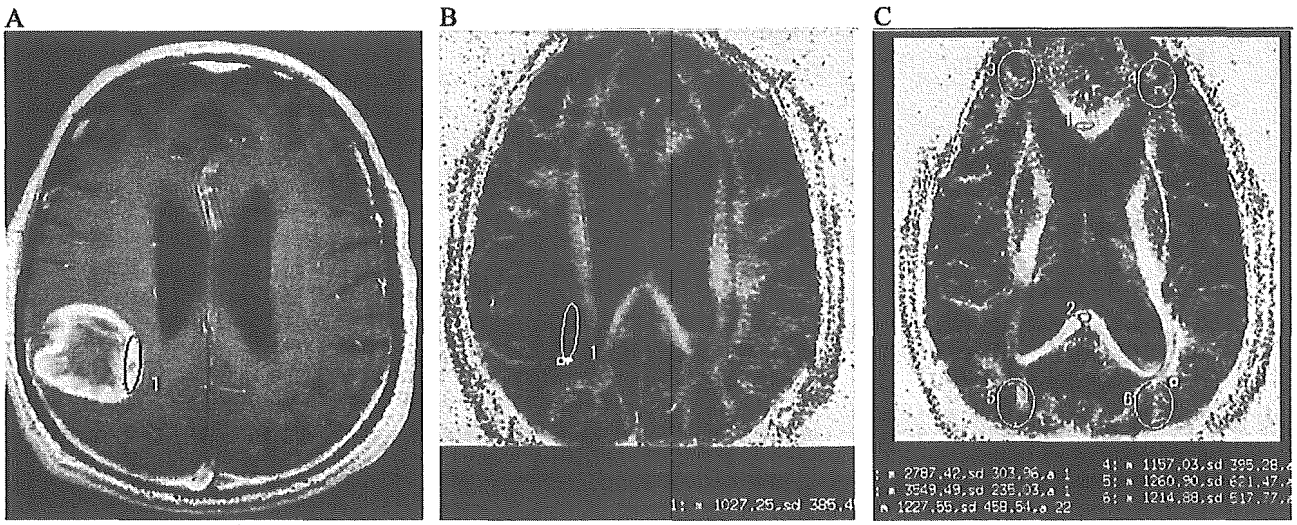

Fig. 1. Locations of ROI in a patient with glioblastoma of the right parietal lobe. A, Gadolinium-enhanced T1-weighted MR image. Circle, ROI within a ring-enhancing lesion of the tumor. B, The coregistered FA maps from DTI. The ROI that was determined from the gadolinium-enhanced T1-weighted MR image was transferred onto a FA map. C, FA map for NWM. Because the tumor was situated in the parietal lobe, only FA values in ROIs of the contralateral frontal lobe (No 4) and the genu (No 1) were accepted.

given ROI. All MRI and DTI procedures were performed by 1 investigator (TI).

2.3. Tumor tissue specimens

In all patients, the tumor tissue specimens were obtained by computed tomography–guided stereotactic biopsy targeted to the intratumoral area corresponding exactly to the ROI within which the FA value was measured. For patients who underwent tumor resection with a large craniotomy, stereotactic biopsy was performed prior to tumor resection. In these patients, a silicon tube was left in the intracerebral trajectory made by the biopsy and was then used as a guide for tumor localization during tumor resection.

After biopsy, specimens were immediately fixed in 30% formalin for 24 hours at room temperature and then embedded in paraffin. Each paraffin block was cut into 6-μm-thick serial sections that were used for hematoxylin and eosin staining and Ki-67 immunohistochemical staining. Cell density was identified as the mean of tumor cell numbers in hematoxylin and eosin–stained preparations in 10 fields of a square 25 μm per side under 200 × magnification. Ki-67 was immunohistochemically detected using anti-Ki-67 monoclonal antibody (MIB-1, DAKO, Copenhagen, Denmark) diluted 1:50 and was stained by the modified avidin-biotin-peroxidase complex method [11]. Prior to Ki-67 immunohistochemical staining, sections were treated in an autoclave at 121°C for 15 minutes. The percentage of stained positive cells in approximately 1000 cells, except for inflammatory cells and vascular cells, under a light microscope (200 ×) was defined as the MIB-1 index for that patient. All histologic analyses were performed by 3 investigators (YS, NY, and AK) with no prior knowledge of the patient data.

2.4. Statistical analysis

Mean FA values of subcortical NWM, normal corpus callosum, and glioblastoma tissue were calculated and then compared statistically using 1-factor ANOVA. Correlation among FA values, cell density, and MIB-1 indices of glioblastoma tissues was analyzed statistically using Pearson's correlation coefficient. Statistical significance was established at the $P < 0.05$ level.

3. Results

The mean FA values of the corpus callosum (the genu in 9 patients and the splenium in 10 patients), subcortical white

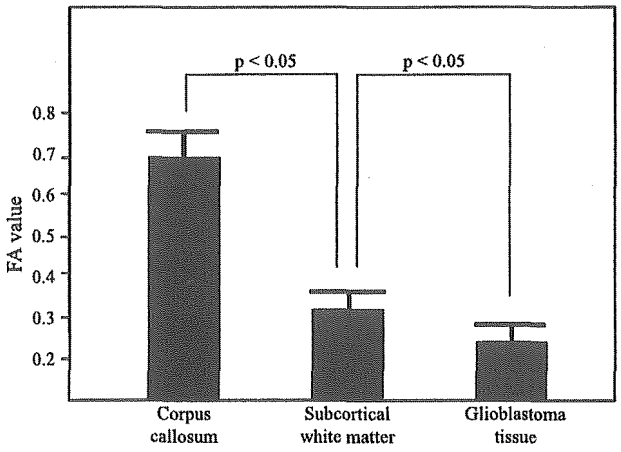

Fig. 2. Mean FA values of regions in NWM and glioblastoma. Significant differences in mean FA values were observed between the corpus callosum, subcortical white matter and glioblastoma lesion.

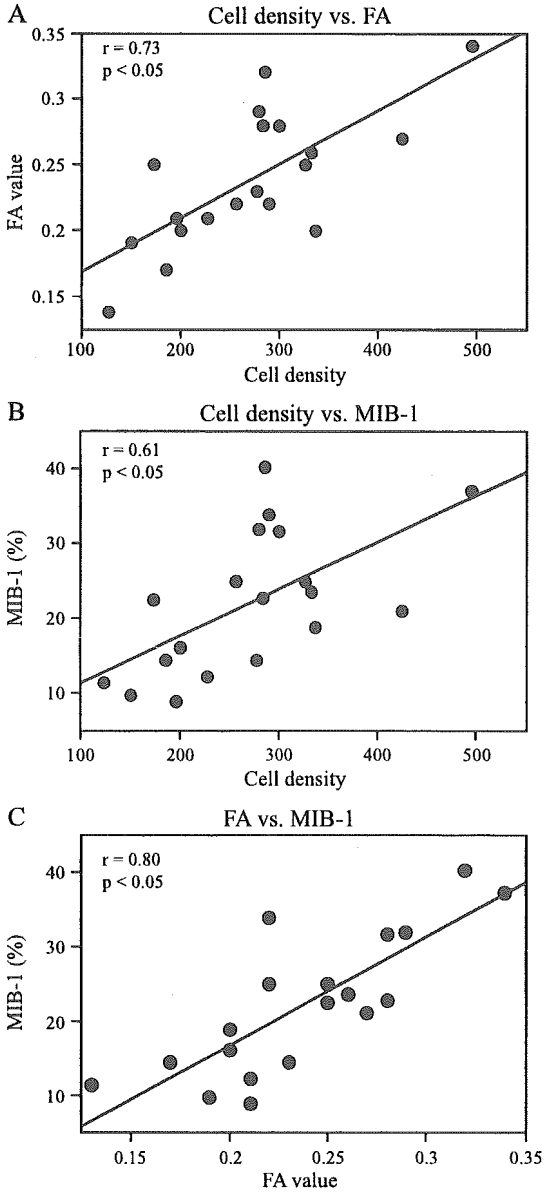

Fig. 3. Correlation between FA value and cell density (A), between cell density and MIB-1 index (B), and between FA value and MIB-1 index (C) in all patients. Strong correlation was observed between FA value and cell density (A) and between FA value and MIB-1 index (C), whereas correlation between cell density and MIB-1 index was moderate (B).

matter (the frontal lobe in 9 patients and the occipital lobe in 10 patients), and glioblastoma lesion were 0.70 ± 0.05, 0.32 ± 0.04, and 0.24 ± 0.05, respectively. The mean FA values were significant different among the corpus callosum, subcortical white matter, and glioblastoma tissue ($P < 0.05$; Fig. 2).

In glioblastoma lesions, the mean values of cell density and MIB-1 index were 270 ± 93% and 21.6 ± 10.0%, respectively. Strong correlation was observed between FA value and cell density ($r = 0.73$, $P < 0.05$) and between FA value and MIB-1 index ($r = 0.80$, $P < 0.05$; Fig. 3A, C), whereas there was moderate correlation between cell density and MIB-1 index ($r = 0.61$, $P < 0.05$; Fig. 3B).

4. Discussion

Normal white matter shows strong directionality of water diffusion and, consequently, a high FA value, because the water diffusion parallel to the white matter tracts is less restricted than the water diffusion perpendicular to them [26]. Although limited information is available for the subcortical NWM and corpus callosum, FA values are 0.2 to 0.6 in the frontal lobe [7,8,21,24,28] and 0.6 to 0.8 in the corpus callosum [1,7,8,16,21]. The FA values in the present study for the subcortical NWM and corpus callosum were similar to those reports (Fig. 2), confirming the reliability of the FA values obtained here. On the other hand, the FA values of glioblastoma tissue have been reported to be lower than those of NWM [20], which is consistent with our result. When astrocytic tumors grow in white matter, almost all normal fiber and cell structures are destroyed by the tumor nidus or displaced and separated to surround the tumor nidus [27]. One possible explanation for the lower mean FA values of the tumor core than NWM is that destruction or displacement of normal fibers induces a decrease in the directionality of water diffusion and a relative decrease in FA value [3,20].

FA value is thought to be largely affected by tumor cell density in glioma tissue [20]. Our preliminary study reported that higher anaplastic grade and higher cell density increased the FA value of differently graded gliomas [3]. The present study indicated that FA values strongly correlated with cell density even when the analysis was limited to glioblastomas alone (Fig. 3A). We hypothesized that the FA value of astrocytic tumor tissue is determined by a balance between factors decreasing the degree of the directionality of water diffusion, such as fiber destruction or displacement, and factors increasing it, such as high cell density and/or vascularity [3]. Even in a study group limited to glioblastomas, cell density rather than normal fiber tracts would predominantly affect FA value, as normal fibers are completely destroyed or displaced to around the tumor core. In the present study, FA value strongly correlated with MIB-1 index (Fig. 3C). This finding could be arrived by syllogism (ie, correlation between FA value and cell density and between cell density and MIB-1 index) and allows the assumption of correlation between FA value and MIB-1 index. The correlation between FA value and MIB-1 index suggests that the FA value predicts not only cell density but also proliferation activity in glioblastomas. Although there is general consensus that MIB-1 index does not allow a prognosis in individual patients with glioblastoma [13], we believe that prediction of proliferation activity prior to surgery would be helpful for the diagnosis and characterization of glioblastomas.

Why FA value, which is an indicator of directionality of water diffusion, correlates strongly with cell density in glioblastoma tissue is unclear. Using diffusion-weighted MRI, evaluations of water diffusion in gliomas or the other

brain tumors have been documented previously [4,5,9,14, 15,22,23]. All authors reported that the value of the apparent diffusion coefficient, which is an indicator of the magnitude of water diffusion, decreased with tumor cell density. The apparent diffusion coefficient values negatively correlated to the cell density in both glioblastomas and diffuse astrocytomas [14]. Furthermore, low apparent diffusion coefficient value in gliomas reflects a decreased volume of extracellular space, which accelerates water diffusion due to encroachment by tumor cells, and/or an increased intracellular viscosity [5,22]. Similarly, we speculate that 1 possible reason for the correlation between FA value and cell density is that an increased amount of cellular membranes and intracellular viscosity, as well as relatively decreased extracellular space in glioblastoma tissue, also induces an increase in the extent of directionality of water diffusion within each pixel of DTI, resulting in a relative increase in FA value.

The present study possesses some limitations regarding interpretation of the FA values. First, how structural factors other than cell density (eg, vascularity, edema, microcysts, tumor cell size, bipolar processes of neoplastic cells, and velocity of flowing blood in capillaries) affect the directionality of water diffusion and alter FA values was not explored. Although the present results suggest that primarily cell density affects FA value, these other factors may also affect it to some small extent. This issue is a matter for future analysis. Second, the present results do not apply to the invading lesion around a tumor nidus. Within such lesions, tumor cells infiltrate along myelinated fibers and disrupt normal cell structure [13]. It is not clear how the directionality of water diffusion and FA are affected by preserved fiber tracts, normal cell structure, and vigorous edema in peritumoral regions. Third, the present results do not apply to brain tumors other than glioblastoma, because the histologic structures of the other tumors differ from those of glioblastoma. For example, the FA value of gliomatosis cerebri with moderate cell density is equivalent to that of glioblastoma, because preservation of normal axons increases the extent of directionality of water diffusion [3]. Correlation of FA value with cell density and proliferation activity is required for each tumor using a study group limited to 1 type.

In conclusion, our findings suggested that the FA value of glioblastoma is determined at the very least by cell density and, consequently, correlates with proliferation activity, although the sample size of the present study was small. Measurement of FA value using DTI will most likely become an option for auxiliary examinations prior to surgery for glioblastoma.

Acknowledgments

This study was supported in part by a grant-in-aid for Advanced Medical Science Research from the Ministry of Science, Education, Sports and Culture, Japan.

References

[1] Bammer R, Augustin M, Strasser-Fuchs S, Seifert T, Kapeller P, Stollberger R, Ebner F, Hartung HP, Fazekas F. Magnetic resonance diffusion tensor imaging for characterizing diffuse and focal white matter abnormalities in multiple sclerosis. Magn Reson Med 2000; 44:583-91.

[2] Basser PJ, Pierpaoli C. Microstructural and physiological features of tissues elucidated by quantitative-diffusion-tensor MRI. J Magn Reson B 1996;111(3):209-19.

[3] Beppu T, Inoue T, Shibata Y, Kurose A, Arai H, Ogasawara K, Ogawa A, Nakamura S, Kabasawa H. Measurement of fractional anisotropy using diffusion tensor MRI in supratentorial astrocytic tumors. J Neurooncol 2003;63:109-16.

[4] Brunberg JA, Chenevert TL, McKeever PE, Ross DA, Junck LR, Muraszko KM, Dauser R, Pipe JG, Betley AT. In vivo MR determination of water diffusion coefficients and diffusion anisotropy: correlation with structural alteration in gliomas of the cerebral hemispheres. AJNR Am J Neuroradiol 1995;16:361-71.

[5] Castillo M, Smith JK, Kwock L, Wilber K. Apparent diffusion coefficients in the evaluation of high-grade cerebral gliomas. AJNR Am J Neuroradiol 2001;22(1):60-4.

[6] Chien D, Kwong KK, Gress DR, Buonanno FS, Buxton RB, Rosen BR. MR diffusion imaging of cerebral infarction in humans. AJNR Am J Neuroradiol 1992;13:1097-105.

[7] Ciccarelli O, Werring DJ, Wheeler-Kingshott CAM, Barker GJ, Parker GJM, Thompson AJ, Miller DH. Investigation of MS normal-appearing brain using diffusion tensor MRI with clinical correlations. Neurology 2001;56:926-33.

[8] Filippi M, Cercignani M, Inglese M, Horsfield MA, Comi G. Diffusion tensor magnetic resonance imaging in multiple sclerosis. Neurology 2001;56:304-11.

[9] Filippi CG, Edgar MA, Ulug AM, Prowda JC, Heier LA, Zimmerman RD. Appearance of meningiomas on diffusion-weighted images: correlating diffusion constants with histopathologic findings. AJNR Am J Neuroradiol 2001;22(1):65-72.

[10] Heesters MA, Koudstaal J, Go KG, Molenaar WM. Proliferation and apoptosis in long-term surviving low grade gliomas in relation to radiotherapy. J Neurooncol 2002;58:157-65.

[11] Hsu SM, Raine L, Fanger H. Use of avidin-biotin-peroxidase complex (ABC) in immunoperoxidase techniques: a comparison between ABC and unlabeled antibody (PAP) procedures. J Histochem Cytochem 1981;29:577-80.

[12] Karamitopoulou E, Perentes E, Diamantis I, Maraziotis T. Ki-67 immunoreactivity in human central nervous system tumors: a study with MIB 1 monoclonal antibody on archival material. Acta Neuropathol (Berl) 1994;87(1):47-54.

[13] Kleihues P, Cavenee WK. World Health Organization classification of tumours: pathology and genetics, tumours of the nervous system. Lyon: International Agency for Research on Cancer (IARC); 2000. p. 6-92.

[14] Kono K, Inoue Y, Nakayama K, Shakudo M, Morino M, Ohata K, Wakasa K, Yamada R. The role of diffusion-weighted imaging in patients with brain tumors. AJNR Am J Neuroradiol 2001;22(6): 1081-8.

[15] Krabbe K, Gideon P, Wagn P, Hansen U, Thomsen C, Madsen F. MR diffusion imaging of human intracranial tumours. Neuroradiology 1997;39(7):483-9.

[16] Melhem ER, Itoh R, Jones L, Barker PB. Diffusion tensor MR imaging of the brain: effect of diffusion weighting on trace and anisotropy measurements. AJNR Am J Neuroradiol 2000;21:1813-20.

[17] Pierpaoli C, Jezzard P, Basser PJ, Barnett A, Di Chiro G. Diffusion tensor MR imaging of the human brain. Radiology 1996;201:637-48.

[18] Pierpaoli C, Basser PJ. Toward a quantitative assessment of diffusion anisotropy. Magn Reson Med 1996;36(6):893-906.

[19] Schroder R, Feisel KD, Ernestus RI. Ki-67 labeling is correlated with the time to recurrence in primary glioblastomas. J Neurooncol 2002; 56:127-32.

[20] Sinha S, Bastin ME, Whittle IR, Wardlaw JM. Diffusion tensor MR imaging of high-grade cerebral gliomas. AJNR Am J Neuroradiol 2002;23(4):520-7.
[21] Sorensen AG, Buonanno FS, Gonzalez RG, Schwamm LH, Lev MH, Huang-Hellinger FR, Reese TG, Weisskoff RM, Davis TL, Suwanwela N, Can U, Moreira JA, Copen WA, Look RB, Finklestein SP, Rosen BR, Koroshetz WJ. Hyperacute stroke: evaluation with combined multisection diffusion-weighted and hemodynamically weighted echo-planar MR imaging. Radiology 1996;199(2):391-401.
[22] Sugahara T, Korogi Y, Kochi M, Ikushima I, Shigematu Y, Hirai T, Okuda T, Liang L, Ge Y, Komohara Y, Ushio Y, Takahashi M. Usefulness of diffusion-weighted MRI with echo-planar technique in the evaluation of cellularity in gliomas. J Magn Reson Imaging 1999;9:53-60.
[23] Tien RD, Felsberg GJ, Friedman H, Brown M, MacFall J. MR imaging of high-grade cerebral gliomas: value of diffusion-weighted echoplanar pulse sequences. AJR Am J Roentgenol 1994;162(3): 671-7.
[24] Tievsky AL, Ptak T, Farkas J. Investigation of apparent diffusion coefficient and diffusion tensor anisotropy in acute and chronic multiple sclerosis lesions. AJNR Am J Neuroradiol 1999;20:1491-9.
[25] Wakimoto H, Aoyagi M, Nakayama T, Nagashima G, Yamamoto S, Tamaki M, Hirakawa K. Prognostic significance of Ki-67 labeling indices obtained using MIB-1 monoclonal antibody in patients with supratentorial astrocytomas. Cancer 1996;77(2):373-80.
[26] Witwer BP, Moftakhar R, Hasan KM, Deshmukh P, Haughton V, Field A, Arfanakis K, Noyes J, Moritz CH, Meyerand ME, Rowley HA, Alexander AL, Badie B. Diffusion-tensor imaging of white matter tracts in patients with cerebral neoplasm. J Neurosurg 2002;97: 568-75.
[27] Yasargil MG. Microneurosurgery IV A [in 4 volumes]. Stuttgart/New York Verlag: Georg Thieme; 1993. p. 127 [for distribution in Japan: Nankodo Company Ltd Tokyo].
[28] Yoshiura T, Wu O, Zeheer A, Reese TG, Sorensen G. Highly diffusion-sensitized MRI of brain: dissociation of gray and white matter. Magn Reson Med 2001;45:734-40.

Commentary

In this interesting article, Beppu et al suggest that diffusion tensor imaging can be used to look at the disruption of fibers by an invasive tumor. This is a potentially important application of this novel technique to the analysis of brain tumors. At the Brigham and Women's Hospital, we have developed this technology primarily to assess to what degree low-grade tumors infiltrate rather than disrupt fibers. It has been an important tool for assessing the likelihood that surgery will cause new deficits in patients with these tumors.

The findings of Beppu et al are what we all might well believe—that glioblastomas are invasive tumors that significantly disrupt normal fiber tracts. Although the study has relatively few patients, the techniques are quite demanding and therefore worthwhile reading. This is a valuable addition to the literature of neurosurgical oncology to decide whether surgery should be done.

Peter M. Black, MD, PhD
Department of Neurosurgery
Children's Hospital
Boston, MA 02115, USA

Journal of Neuro-Oncology (2005) 73: 137–144
DOI 10.1007/s11060-004-3340-4

Clinical Study

Utility of three-dimensional anisotropy contrast magnetic resonance axonography for determining condition of the pyramidal tract in glioblastoma patients with hemiparesis

Takaaki Beppu[1], Takashi Inoue[1], Yasutaka Kuzu[1], Kuniaki Ogasawara[1], Akira Ogawa[1] and Makoto Sasaki[2]
[1]*Department of Neurosurgery;* [2]*Department of Radiology, Iwate Medical University, Morioka, Japan*

Key words: glioblastoma, pyramidal, tract, axonography,diffusion MRI

Summary

Background and purpose: Three-dimensional anisotropy contrast magnetic resonance axonography (3DAC) is a technique for diffusion weighted magnetic resonance imaging (DWI) that offers reliable visualization of the pyramidal tracts. This study evaluated condition of the pyramidal tract using 3DAC in glioblastoma patients with hemiparesis. *Methods:* In 18 glioblastoma patients before surgery, 3DAC findings of the pyramidal tract responsible for hemiparesis were compared with finding from proton density-weighted imaging (PDWI). To estimate extent of pyramidal tract destruction, fractional anisotropy (FA) values using diffusion tensor magnetic resonance imaging were examined for both the responsible and non-pathological pyramidal tracts. *Results*: In all five patients for whom PDWI indicated no hyperintense foci in the responsible pyramidal tract, 3DAC demonstrated no change in color. When PDWI revealed hyperintense foci, 3DAC showed two types of findings: no color change (five patients); or obscured dark area (six patients). When 3DAC showed a dark area, mean FA value in the responsible tract was significantly lower than that for the non-pathological tract. *Conclusion:* When PDWI indicates hyperintense foci on the pyramidal tract, 3DAC allows prediction of pyramidal tract condition, such as large tumor invasion.

Introduction

Developments in neuroimaging technology have enabled accurate preoperative evaluation of cerebral cortical function and integrity [1–5]. Evaluation of subcortical integrity is also necessary prior to surgery, as functional recovery after surgery may be limited by previous subcortical injury [6,7]. For example, decisions regarding surgical approach and predictions of individual performance status after surgery vary according to the cause of subcortical functional disorder, such as compression, invasion, or disruption of the subcortical tracts by glioma.

Diffusion-weighted imaging (DWI) and diffusion tensor imaging (DTI) are magnetic resonance imaging (MRI) techniques that provide quantitative information about the magnitude and direction of water diffusion, respectively, in a three-dimensional space. These techniques offer some advantages for evaluating subcortical structures comprising white matter tracts, since diffusion of water parallel to nerve fibers is less restricted than water diffusion perpendicular to the fibers [8–10]. Using DWI and DTI, the corticospinal tracts can be visualized as 'tractography' [11–16]. Three-dimensional anisotropy contrast magnetic resonance axonography (3DAC) using DWI is one method of tractography, and represents a reliable technique for visualizing anisotropic diffusion through nerve fibers [17,18]. Of the cerebral white matter nerve fiber tracts, the pyramidal tract is particularly suitable for 3DAC [18]. Currently, 3DAC allows clinical estimation of pyramidal tract status in patients with cerebral infarction or brain tumor [14,15,19,20]. In patients with glioma, tractography provides information on the localization of tumor bulk relative to the pyramidal tract. This useful information has been utilized in the field of brain tumor surgery [21–24]. When a tumor attaches to the pyramidal tract in a patient with hemiparesis, information on condition of the pyramidal tract adjacent to the tumor, such as compression, invasion or disruption by the tumor, is often desired for glioma resection. If 3DAC could provide not only information on localization of tumor bulk and the pyramidal tract, but also condition of the pyramidal tract, 3DAC would become even more useful for neuro-oncologists.

Proton density-weighted imaging (PDWI) on conventional MRI can obtain a high contrast between gray and white matter, and is used for visualization of the corticospinal tracts [25]. We compared PDWI findings in the pyramidal tract responsible for hemiparesis with findings from 3DAC. Furthermore, fractional anisotropy (FA) value was measured to estimate extent of the pyramidal tract destruction. FA value from DTI provides the best quantitative information regarding degree of directionality of water diffusion, and can thus indicate degree of nerve fiber destruction [16,26,27]. The present study aimed to determine the utility of 3DAC for estimating condition of the pyramidal tracts in patients with hemiparesis due to glioblastoma, and to define patient subgroups that would benefit from 3DAC.

Methods

Patients and clinical course

The study protocol was approved by the Ethics Committee of Iwate Medical University, Morioka, Japan. Patients recruited to this study were admitted to the Department of Neurosurgery at Iwate Medical University between September 2000 and March 2004. Entry criteria for this study were: adult (20 years old) patients who had been diagnosed with supratentorial glioblastoma mainly sited in the cerebral white matter excluding the primary motor cortex and brain stem; patients who presented with hemiparesis due to motor-related disorder of the pyramidal tract; and provision of written informed consent to participate. Diagnosis of glioblastoma was based on histological features of surgical specimens obtained after processing all image analyses. Patient data are summarized in Table 1. Subjects comprised 18 patients (six males, 12 females) with a mean age of 58.5 years (range, 31–77 years). Twelve patients were treated using either total or subtotal tumor removal, and six patients underwent only biopsy. Extent of hemiparesis before and after surgery was evaluated for the arm, finger and foot of each patient using Bruunstrom's grading system [28]. This system utilizes six stages, with stage 1 equal to severe hemiplegia and stage 6 representing basically normal strength. The lowest stage from the arm, finger or foot was used to define degree of hemiparesis for each patient. All patients underwent radiochemotherapy starting from 2 weeks after surgery. Postoperative hemiparesis was evaluated immediately before starting radiochemotherapy. Hemipareses before and after surgery were compared statistically. Values of $P < 0.05$ were considered statistically significant.

Conventional MRI

Conventional MRI was performed within 7 days before surgery. All patients underwent fast spin-echo PDWI and T2-weighted imaging (WI), and conventional spin-echo non-enhanced and gadolinium-enhanced T1-WI (Gd-T1WI) prior to DWI. Conventional MRI was performed using a 1.5-T whole body scanner (GE Yokogawa Medical Systems, Tokyo, Japan) and standard head coil. The pyramidal tract nearest the tumor on PDWI was defined as the tract responsible for hemiparesis. Estimations of the responsible tract using conventional MRI were performed using the criteria outlined below. Responsible tracts were classified into three groups according to PDWI: (1) 'clear' group in which tracts were clearly visualized without hyperintense foci; (2) 'hyperintense' group in which tracts displayed hyperintense foci; and (3) 'absent' group in which tracts could not be observed due to heavy compression or involvement with a large tumor. Observation in the responsible tract was performed at a region without enhancement on Gd-T1WI.

Imaging by 3DAC

All 3DAC scans were performed within 7 days before surgery. DWI scans were performed using a 3.0-T MRI system (Signa VH/I; GE Medical Systems, Milwaukee, WI, USA) using a standard head coil. A spin echo-type echo planar imaging sequence with diffusion gradients applied in three directions was used for DWI (repetition time (TR), 8000 ms; echo time (TE), 93 ms; matrix 128 × 128; field of view (FOV), 240 × 240 mm; 5 mm thickness; b factors, 1000 s/mm^2). The 3DAC image analysis after processing was performed in accordance with the methods described by Inoue et al. [19,20]. Images obtained using left-right, anterior-posterior and superior-inferior diffusion gradients were first transformed into grayscale levels, then color-coded using red, green, and blue, respectively. Colored images were then composited into a single colored image. Identical intensities of three colors, indicating isotropic diffusion, combined on images to appear as cancellation (white-out). In contrast, non-identical intensities of the three

Table 1. Patient characteristics

Case	Age/Sex	Tumor site	Hemiparesis Pre-op	Procedure	Hemiparesis Post-op
1	77 F	Lateral ventricle	3	biopsy	3
2	70 M	Corpus callosum	5	biopsy	5
3	70 M	Corpus callosum	4	biopsy	2
4	69 F	Parietal lobe	2	total	5
5	67 F	Parietal lobe	5	total	5
6	67 F	Parietal lobe	5	total	5
7	66 F	Frontal lobe	5	total	4
8	65 M	Parietal lobe	3	total	3
9	64 F	Basal ganglia	3	biopsy	2
10	64 M	Parietal lobe	5	total	5
11	63 M	Temporal lobe	5	total	5
12	63 F	Frontal lobe	5	total	6
13	56 F	Frontal lobe	4	biopsy	4
14	54 F	Frontal lobe	5	total	4
15	47 M	Temporal lobe	5	total	6
16	44 F	Corpus callosum	3	biopsy	2
17	41 F	Thalamus	5	subtotal	6
18	31 F	Frontal lobe	1	subtotal	5

Total, total removal; Subtotal, subtotal removal; Pre-op, preoperative; Post- op, postoperative.

colors, which are indicative of anisotropic diffusion, appear as the color showing the greatest strength and direction of the diffusion gradient. Thus, nerve fibers running left-right (x-axis), anterior-posterior (y-axis) and superior-inferior (z-axis) appear as green, blue and red, respectively. Mixed colors indicate oblique orientation of nerve fibers.

On 3DAC images, the same region of the pyramidal tract as the responsible tract defined on PDWI was observed in all patients, and patients were classified into three groups: (1) 'fine' group, in which the tract was observed without any change in color, compared with the pyramidal tract on the contralateral side of the same slice; (2) 'dark' group, in which color of the tract was obscure and dark; and (3) 'absent' group, in which tract could not be observed due to strong compression or involvement with a large tumor bulk.

FA value

DTI was performed using a 3.0-T MRI system (Signa VH/I; GE Medical Systems) with a standard head coil. A spin echo type echo planar imaging sequence with diffusion gradients applied in six directions was used for DTI (TR, 10,000 ms; TE, 84 ms; matrix, 256 × 260; FOV, 240 mm^2; 6 mm thickness, 2 mm gap; b factors, 800 s/mm^2). All patients also underwent conventional spin echo T1- and T2-WI prior to DTI, and T1WI with contrast medium after DTI. All image analyses after processing were performed on a scanner console using a subprogram of the Functool™ image analysis software (General Electric Medical Systems, Buc, France).

The FA values were measured at pyramidal tracts of the pathological and non-pathological sides. Regions of interest (ROI) were placed at the same region of the pyramidal tract as the responsible tract estimated on PDWI and 3DAC, and at the symmetrical region on the pyramidal tract of the non-pathological side. ROIs were automatically transferred onto co-registered FA maps constructed from DTI. FA values were then calculated for each patient using the modified Functool image analysis software. FA value was identified as the mean of values derived for every pixel in a given ROI. Statistical significance was established at the $P < 0.05$ level in all analyses.

Results

Findings of PDWI and 3DAC (Table 2)

The tract responsible for hemiparesis was the corona radiata in 14 patients, and the internal capsule in four patients. On PDWI, the finding of 'clear' in the responsible tract was observed in five patients. Responsible tracts in 11 patients revealed findings of 'hyperintense'. On 3DAC, the responsible tract was 'fine' in 10 patients and 'dark' in six. The tract in two patients displayed findings of 'absent' for both PDWI and 3DAC. All patients for whom PDWI showed findings of 'clear' demonstrated finding of 'fine' on 3DAC. When PDWI showed 'hyperintense', 3DAC demonstrated either 'fine' or 'dark'. As a result, patients could be classified into four groups (Table 2): Group A, 'clear' on PDWI and 'fine' on 3DAC ($n = 5$, 28%); Group B, 'hyperintense' on PDWI and 'fine' on 3DAC ($n = 5$, 28%); Group C, 'hyperintense' on PDWI and 'dark' on 3DAC ($n = 6$, 33%); and Group D, 'absent' on both procedures ($n = 2$, 11%).

Illustrative cases

Case 17 – Group A: The internal capsule was the tract responsible for hemiparesis, revealing 'clear' findings without hyperintense foci on PDWI, and 'fine' without any change in color compared to the contralateral side on 3DAC (Figure 1a–c).

Table 2: Findings of PDWI, 3DAC and FA

Case	Responsible tract	PDWI	3 DAC	Group	FA value	
					Non-pathological tract	Responsible tract
1	Corona radiata	Hyperintense	Fine	B	0.76	0.61
2	Corona radiata	Hyperintense	Dark	C	0.82	0.65
3	Corona radiata	Hyperintense	Dark	C	0.50	0.17
4	Corona radiata	Hyperintense	Fine	B	0.58	0.38
5	Corona radiata	Clear	Fine	A	0.57	0.54
6	Corona radiata	Hyperintense	Fine	B	0.52	0.45
7	Corona radiata	Hyperintense	Dark	C	0.69	0.23
8	Corona radiata	Hyperintense	Dark	C	0.65	0.36
9	Internal capsule	Hyperintense	Dark	C	0.56	0.39
10	Corona radiata	Hyperintense	Fine	B	0.62	0.66
11	Internal capsule	Clear	Fine	A	0.68	0.64
12	Corona radiata	Absent	Absent	D	0.77	0.53
13	Corona radiata	Clear	Fine	A	0.77	0.73
14	Corona radiata	Hyperintense	Dark	C	0.62	0.26
15	Internal capsule	Clear	Fine	A	0.65	0.67
16	Corona radiata	Hyperintense	Fine	B	0.67	0.65
17	Internal capsule	Clear	Fine	A	0.62	0.55
18	Corona radiata	Absent	Absent	D	0.49	0.46

Case 10 – Group B: In this case, the corona radiata was the responsible tract, displaying findings of 'hyperintense' on PDWI, and 'fine' on 3DAC (Figures 2a–c).

Case 7 – Group C: The corona radiata was the responsible tract, displaying findings of 'hyperintense' on PDWI, and 'dark' on 3DAC (Figure 3a–c). The patient underwent gross total removal of tumor bulk. Gd-T1WI at 3 months after surgery revealed a recurrent lesion in the same region as the slight dark lesion on initial 3DAC (Figure 4a), and 3DAC identified a black lesion in the area corresponding to the Gd-enhanced lesion (Figure 4b).

Case 18 – Group D: The corona radiata was the responsible tract, but could not be observed on either PDWI or 3DAC (Figure 5a–c).

FA value

Mean FA value of the pyramidal tract on the non-pathological side was 0.64 ± 0.10 (range, 0.49–0.77). In the responsible tracts, FA value ranged widely from 0.17 to 0.73 (Table 2). Comparison between FA values of non-pathological tract and responsible tract for each group was performed using paired *t*-tests. No significant

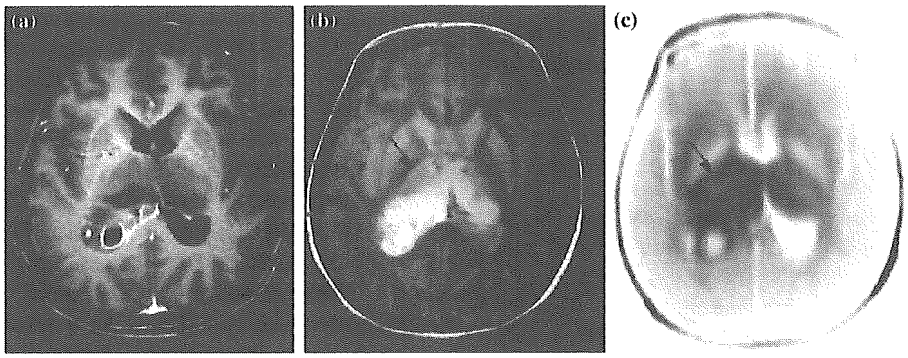

Figure 1. Conventional MRI and 3DAC in Case 17. (a) Gd-T1WI demonstrates glioblastoma situated in the right thalamus. (b) PDWI clearly shows the internal capsule as the tract responsible for hemiparesis, ipsilateral to the tumor (arrow). (c) Internal capsule is shown on 3DAC by absence of color change compared to contralateral side (arrow).

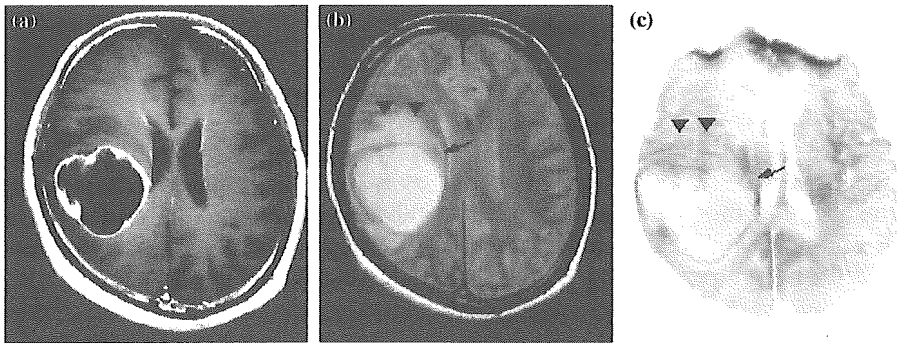

Figure 2. Conventional MRI and 3DAC in Case 10. (a) Gd-T1WI demonstrates a cystic-shaped glioblastoma situated in the right parietal lobe. (b) PDWI shows a hyperintense focus in the corona radiata as the responsible tract (arrow), and subcortical white matter surrounding the tumor, suggesting a perifocal edema (arrowhead). (c) 3DAC demonstrates no change in color for both corona radiata (arrow) and subcortical white matter surrounding the tumor, corresponding to a hyperintense focus on PDWI (arrowhead). Fluid within the cystic lesion is shown as an area of whiteout, as is cerebrospinal fluid within the lateral ventricle.

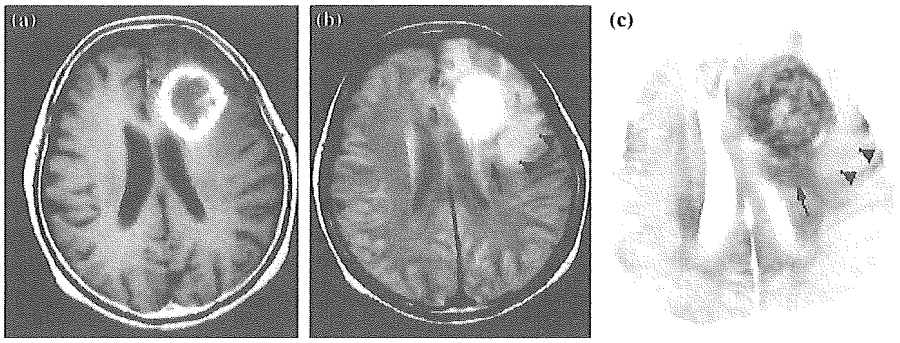

Figure 3. Conventional MRI and 3DAC in Case 7. (a) Gd-T1WI shows glioblastoma situated in the left frontal lobe. (b) PDWI demonstrates hyperintense foci, with corona radiata behind the tumor bulk (arrow), as the responsible tract, and subcortical white matter surrounding the tumor bulk (arrowhead). (c) 3DAC demonstrates slight darkness on the corona radiata (arrow), whereas white matter surrounding the tumor bulk displays faint coloration (arrowhead). The tumor bulk is darker than the responsible tract.